Synergistic Interactions between Urban Heat Islands and Heat Waves: The Impact in Cities Is Larger than the Sum of Its Parts*

DAN LI AND ELIE BOU-ZEID

Department of Civil and Environmental Engineering, Princeton University, Princeton, New Jersey

(Manuscript received 20 December 2012, in final form 17 April 2013)

ABSTRACT

Cities are well known to be hotter than the rural areas that surround them; this phenomenon is called the urban heat island. Heat waves are excessively hot periods during which the air temperatures of both urban and rural areas increase significantly. However, whether urban and rural temperatures respond in the same way to heat waves remains a critical unanswered question. In this study, a combination of observational and modeling analyses indicates synergies between urban heat islands and heat waves. That is, not only do heat waves increase the ambient temperatures, but they also intensify the difference between urban and rural temperatures. As a result, the added heat stress in cities will be even higher than the sum of the background urban heat island effect and the heat wave effect. Results presented here also attribute this added impact of heat waves on urban areas to the lack of surface moisture in urban areas and the low wind speed associated with heat waves. Given that heat waves are projected to become more frequent and that urban populations are substantially increasing, these findings underline the serious heat-related health risks facing urban residents in the twenty-first century. Adaptation and mitigation strategies will require joint efforts to reinvent the city, allowing for more green spaces and lesser disruption of the natural water cycle.

1. Introduction

Heat waves (HWs) are among the deadliest natural disasters: the 2003 European episode is estimated to have resulted in up to 70 000 deaths on the continent (Robine et al. 2008). The Intergovernmental Panel on Climate Change projects that the frequency of HWs is likely to increase over most land areas in the twenty-first century (Solomon et al. 2007). In the United States, HWs are expected to become more intense, more frequent, and longer lasting (Meehl and Tebaldi 2004). Epidemiological studies have found a 4.5% increase in mortality risk for every 1°C increase in heat wave intensity, and a 0.38% increase for every 1-day increase in heat wave duration in the United States (Anderson and Bell 2011). Cities are more vulnerable to heat waves than rural areas because of the preexisting urban heat island (UHI) effect; that is, cities are generally warmer than the surrounding rural areas (Oke 1982; Grimmond 2007). In addition, more than 50% of the world population is currently living in cities, and this percentage is projected to continue growing rapidly (Grimm et al. 2008). This combination of anthropogenic and natural factors makes the temperature response to heat waves in cities of great importance for human health and well-being.

There is no unified definition of a heat wave (Meehl and Tebaldi 2004); in this study, a heat wave is identified as a sustained period of excessively hot days during which the temperature is significantly higher than the average climatological mean. A heat wave typically results from large-scale, stagnant, high pressure systems that produce a temporal temperature anomaly for an entire region; therefore, heat waves increase the air temperature and, concomitantly, the surface temperature for both urban and rural areas. On the other hand, the UHI is recognized as a local effect, which is primarily due to the characteristics of urban terrain, including lower albedo (partially due to radiative trapping effects), higher heat capacity, limited green spaces, and significant anthropogenic heat releases (Oke 1982). The UHI thus produces a permanent spatial temperature anomaly concentrated

* Supplemental information related to this paper is available at the Journals Online website: http://dx.doi.org/10.1175/JAMC-D-13-02.s1.

Corresponding author address: Dan Li, Dept. of Civil and Environmental Engineering, Princeton University, Princeton, NJ 08540.
E-mail: danl.princeton.2009@gmail.com

DOI: 10.1175/JAMC-D-13-02.1

over cities, whose strength is measured by the so-called UHI index ΔT, defined as the difference between the urban and rural air (or surface) temperatures.

Potential interactions or synergies between the two phenomena, which determine whether the UHI index will be intensified or weakened by HWs, remain elusive and that is despite the substantial and extensive implications of such interactions. There are a number of physical attributes of UHIs and HWs that might shed some light on the possible ways in which they can interact:

1) Heat waves could strengthen secondary circulations. The hotter air over the city tends to rise, drawing cooler air from the surrounding areas and acting as a negative feedback on the UHI strength (Ohashi and Kida 2002; Hidalgo et al. 2010). For coastal cities, since the sea surface temperature is steady, the higher urban surface temperatures during heat waves may significantly intensify these secondary circulations and lead to cooling by sea breeze (Lebassi et al. 2009, 2011).
2) Heat waves resulting from persistent high pressure anticyclones are usually associated with low wind speeds (Ackerman and Knox 2012). At low wind speeds, the UHI effect is expected to be stronger due to the reduced advective cooling by low-temperature air from surrounding rural areas. Reduced wind speed is thus a likely synergistic factor that can exacerbate the combined UHI and heat wave effects (Oke 1982). However, reduced wind speed also reduces the magnitude of the surface heat flux over cities so its indirect effects on air temperature may result in negative feedbacks that offset the reduced advective cooling.
3) Higher surface temperatures during heat waves will shift the incoming radiative energy partitioning [Eq. (1)] at the surface in favor of more evapotranspiration (LE) and more ground/stored heat flux G (Bateni and Entekhabi 2012), following the surface energy budget equation (written for an infinitesimally thin layer at the surface–atmosphere interface rather than for the whole urban layer):

$$R_n = H + \mathrm{LE} + G. \qquad (1)$$

In Eq. (1), R_n is the net radiation (this is the driving energy flux at the earth surface), H is the sensible heat flux from the surface to the adjacent air, LE is the latent heat flux into the atmosphere from evapotranspiration, and G is the heat flux into the ground surface. All variables are in units of watts per square meter. The potential increase in evaporation during heat waves will reduce the sensible heat flux H, which is the main heat source for warming the air and producing the UHI effect. However, this reduction will be more efficient in rural areas due to the higher availability of surface moisture, thus potentially increasing the urban–rural contrast in surface and air temperatures. As for the increased stored heat G, it will be released during nighttime or on subsequent days, thus changing the timing of peak temperatures.

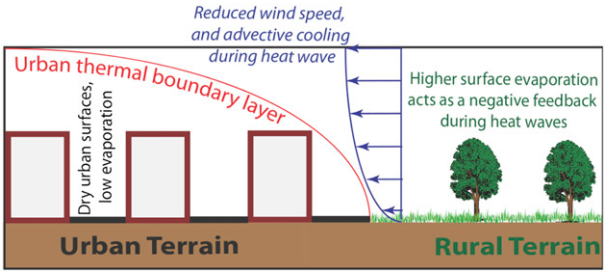

FIG. 1. Synergistic interaction mechanisms between the UHI and HWs, which are mainly related to the reduced moisture availability in urban areas and the reduced wind speed during heat waves.

In essence, the first and second interaction hypotheses are linked to wind speed effects, while the third is tied to the moisture availability difference between urban and rural surfaces. The second and third interaction hypotheses lead to synergistic interactions that exacerbate the heat stress in cities, as illustrated in Fig. 1. The question of which interactions will dominate remains open, but extremely critical (Basara et al. 2010; Tan et al. 2010; Zhou and Shepherd 2010; Fischer et al. 2012). In this study, the interactions between the UHI effect and a heat wave event (from 7 to 10 June 2008) in the Baltimore, Maryland–Washington, D.C., metropolitan area are studied using a unique combination of approaches. For the first time, we are able to identify the dominant mechanisms connecting HWs and UHIs, and to elucidate the physical processes controlling them. High-resolution mesoscale weather simulations, remotely observed land surface skin temperatures, and in situ air temperature measurements are combined to test the following hypothesis: UHIs and HWs interact synergistically and nonlinearly to produce heat stress conditions in cities that are more adverse than a simple addition of the two effects, thus significantly increasing the vulnerability of cities to HWs and climate change. Finally, a simple analytical model, based on a balance between horizontal advection and vertical turbulent diffusion, and coupled to the surface energy budgets [Eq. (1)] over urban and rural areas, is developed to capture the main interactions and to generalize the findings to other heat waves and other urban areas. The analytical model captures the impact of wind speed, surface available moisture, and surface available

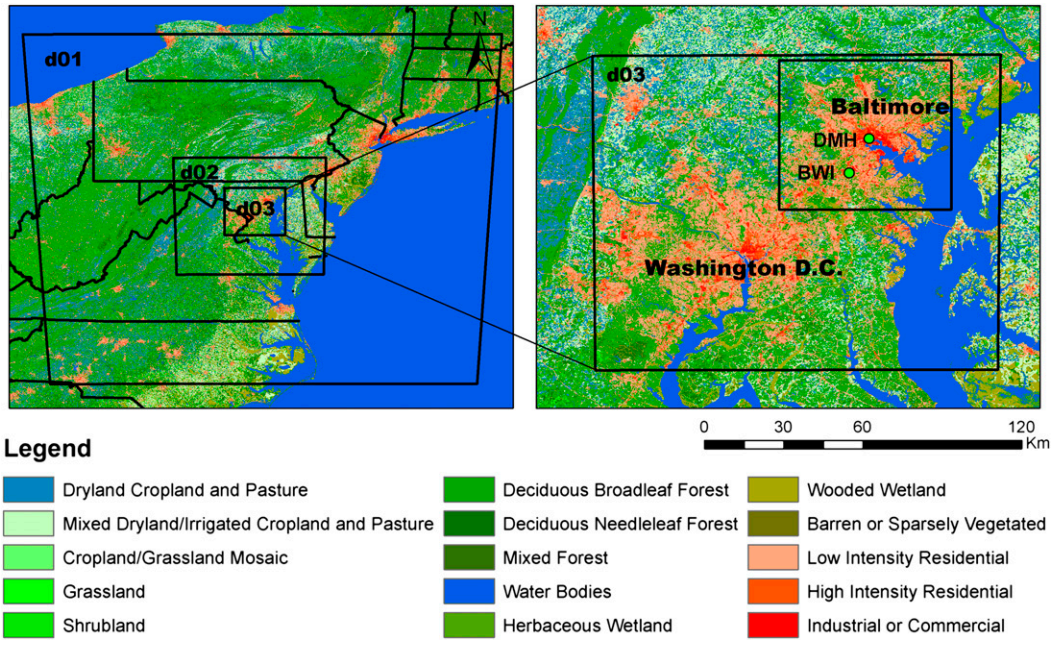

FIG. 2. The land-cover map, the WRF domains, and the observational sites over the study area. The black square centered over Baltimore is the area within which spatially averaged urban and rural air/surface temperatures are computed based on the underlying land-use category (water surface excluded).

energy on the urban microclimate during a heat wave. Other urban processes such as anthropogenic heat emissions (Sailor 2011) and the additional reduction in wind speed due to higher urban surface roughness (Bou-Zeid et al. 2009) are also very important for urban microclimates and thermal comfort, but their impacts are not significantly affected by the presence of a heat wave and, thus, for the purpose of the diagnostic analytical model, we consider them to be part of the background UHI.

2. Research methods: Models and observational datasets

a. WRF model description and setup

In this study, the Weather Research and Forecasting (WRF) model (Skamarock and Klemp 2008) is used to study the urban heat island effect throughout a heat wave period. The WRF model is a mesoscale numerical weather prediction system that has been extensively used to study urban micrometeorology and hydrometeorology due to its nesting capability, which allows high-resolution simulations, and due to the coupled urban canopy models available in WRF (Chen et al. 2011). The current single-layer urban canopy model (UCM), coupled with the Noah land surface model in WRF, can represent three types of urban facets (roof, wall, and ground). In addition, the WRF–Noah–UCM framework distinguishes three urban categories: low-density residential, high-density residential, and commercial. For each urban category, a certain fraction of vegetated surfaces in an urban grid cell is assigned: 50% for low-density residential, 10% for high-density residential, and 5% for commercial; the remainder is the built fraction.

The UCM has been shown to be critical for reproducing the correct surface temperature patterns and air temperatures in the urban areas (Zhang et al. 2011). As such, and before performing the simulations shown below in section 3, we implemented an improved UCM into WRF, which is more accurate than the default available option due to 1) its ability to simulate subfacets consisting of different materials (ground surface, e.g., can be a combination of asphalt, concrete, and urban grass); 2) its more realistic representation of hydrologic processes in the urban canyon, which are very critical to the performance of urban models (Grimmond et al. 2010, 2011); and 3) its use of urban material properties calibrated for the northeastern United States. The full details of the new UCM and the material properties calibration can be found in Wang et al. (2011a,b, 2012).

The WRF simulations in this work are performed over the Baltimore–Washington metropolitan area using three nested domains with horizontal grid spacings of 9, 3, and 1 km. As shown in Fig. 2, the largest domain (d01) covers most of the northeastern United States; d02 includes

Delaware, most of Maryland, and parts of West Virginia and Virginia; and d03 covers the Baltimore and Washington metropolitan areas. All the analyses are conducted using simulated results from d03. For instance, the spatially averaged urban air/surface temperatures are the averaged air/surface temperatures over all urban pixels over Baltimore in d03. The three domains have 100, 121, and 121 horizontal grid cells, respectively, in both the x and y directions. In the vertical direction, 109 grid cells are used in order to resolve the boundary layer structure. The initial and boundary conditions are taken from the North American Regional Reanalysis (details can be found online at http://www.emc.ncep.noaa.gov/mmb/rreanl/ and on http://dss.ucar.edu/datasets/ds608.0/), and the simulations are all started at 0000 UTC 2 June 2008 and ended at 0000 UTC 18 June 2008, with an output frequency of 2 h. The land-use map is taken from the National Land Cover Data (NLCD) for 2006 (Fry et al. 2011), which includes the three urban categories that are needed by the UCM. Some other physical parameterization schemes that are selected and not changed include 1) the Rapid Radiative Transfer Model scheme for longwave radiation, 2) the Dudhia scheme for shortwave radiation, 3) the 2D Smagorinsky scheme for horizontal diffusion, 4) the Noah land surface model, and 5) the Mellor–Yamada–Janjić planetary boundary layer scheme. Cumulus parameterization was not used for any of these domains since even the largest grid size is less than 10 km and there is no rainfall during the simulation period. In addition, one-way nesting is used since all analyses focus on d03.

In this study, 2-m air temperature and surface temperature are investigated. Air temperature at 2 m is widely recognized as a key indicator for the UHI effect since it can directly influence human comfort, while surface temperature is an equally important indicator due to its contribution to the radiative component of thermal comfort. Both also have a direct impact on building energy consumption. Nonetheless, the urban heat island index is different depending on whether the air or surface temperature is used. To provide a comprehensive understanding of the interactions between urban heat islands and heat waves, both air temperature and surface temperature are examined in our analysis. In addition, we define the daytime-averaged temperature at a given location as the mean value of air temperatures above the 50th percentile during a given day, and the nighttime-averaged temperature as the mean value of air temperatures below the 50th percentile. The WRF-simulated air/surface temperature contrasts between urban and rural areas are spatially averaged over the Baltimore metropolitan area (part of d03; see Fig. 2) in order to provide a broader and more spatially representative comparison. The urban and rural areas are identified using the dominant land-use category in the WRF grid cells. The urban areas include grid cells that are dominated by any of the three urban categories, while rural areas are those dominated by other types of surfaces (not including water surfaces).

b. Observational datasets and WRF model evaluation

First, the 2-m air temperatures from WRF are validated using measurements from the Automated Surface Observing System sensors (http://www.nws.noaa.gov/asos/) at the Maryland Science Center (DMH) in downtown Baltimore and at the Baltimore/Washington International Airport (BWI). The locations of the two sites can be found in Fig. 2. Based on the NLCD2006 dataset, the grid cell that DMH is located in has a large urban surface fraction. The fractions of low-density residential, high-density residential, and commercial urban surfaces at the DMH site are 4%, 39%, and 42%, respectively. The rest is water surface (15%). The BWI meteorological station, on the other hand, lies in a grid cell with a significant portion of low-density residential urban land (35%), but is dominated by deciduous broadleaf forest (40%). The BWI site also has 10% deciduous needleleaf forest. As such, the DMH and BWI sites broadly represent an urban site and a suburban–rural site, respectively.

Figure 3 compares the WRF-simulated 2-m air temperatures to the observations at the DMH and BWI sites. This temperature is measured directly by the meteorological stations, while in WRF it is a diagnostic output (the lowest grid point in WRF is at about 25 m). The WRF model with the new UCM reproduces the 2-m air temperature fairly accurately. This is consistent with previous studies that also reported that WRF can adequately simulate the diurnal cycle of 2-m air temperature (Zhang et al. 2011; Talbot et al. 2012; Li et al. 2013). The mean biases are -1.6 and -1.2 K for the DMH and BWI, respectively. The root-mean-square errors (RMSEs) are 2.2 and 2.0 K, respectively. Although some biases are observed in the WRF-simulated 2-m air temperature, the biases are generally of the same sign for urban and suburban–rural sites and will hence partially cancel each other when the urban–rural differences are computed. Consequently, the WRF model with the improved UCM is an adequate tool for investigating the urban–rural contrasts of air temperature (i.e., the urban heat island effect).

In Fig. 4, the surface temperature map produced by WRF is compared with the Moderate Resolution Imaging Spectroradiometer (MODIS) satellite observations; this analysis is similar to those by Leroyer et al. (2011) and Zhang et al. (2011). The MODIS product used in our study is the MYD11A1 version-5 level-3 land surface temperature product. The MODIS-measured surface

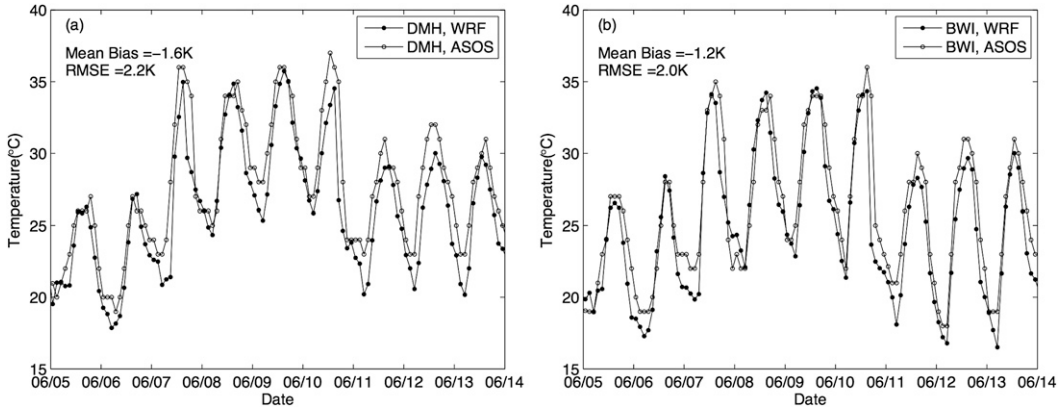

FIG. 3. Comparison between WRF-simulated and observed 2-m air temperatures at (a) DMH and (b) BWI for the period from 5 to 14 June.

skin temperature is available twice a day: once during daytime and once during nighttime. Here, we choose to use the MODIS-measured daytime surface temperature (around 1255 local solar time) on 9 June because of the good data quality resulting from clear skies. As can be seen in Fig. 4, the WRF model with the improved UCM can reproduce the surface temperature pattern observed by the satellite reasonably well. The improvements over simulations with the default UCM, not shown here, are significant (see also Zhang et al. 2011). The differences between WRF-simulated and remotely sensed land surface temperatures are less than 2°C for all land-use categories that cover at least 5% of domain 3 (not shown); these biases are comparable to the uncertainty of the MODIS land surface temperature product (Wan 2008). As a result, the WRF-simulated land surface temperatures are considered sufficiently accurate for our analyses.

c. *An analytical model*

To unravel the physical mechanisms that are responsible for the interactions between urban heat islands and heat waves, a simple analytical model is developed in this study. The analytical model is based on previous work by Yeh and Brutsaert (1971a,b) that solves the turbulent heat and water vapor transfer between a water surface of limited extent and the atmosphere. Our model examines heat and water vapor exchanges between the urban surface and the atmosphere in a two-dimensional domain by coupling the surface energy budget with simplified advection-diffusion equations for thermal energy

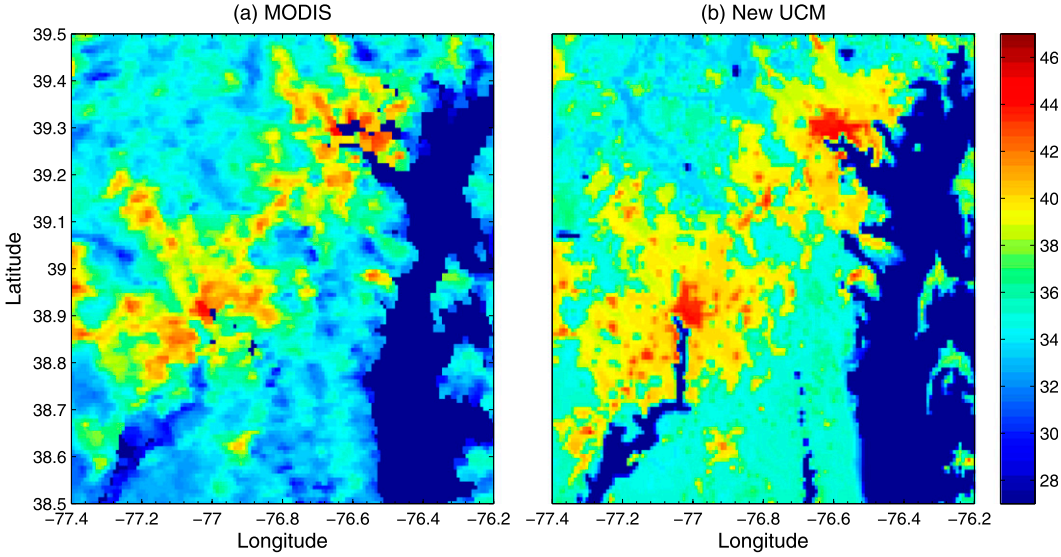

FIG. 4. Comparison between (a) MODIS-observed land surface temperature (°C) and (b) WRF-simulated temperature at 1755 UTC (1255 local solar time) on 9 Jun 2008.

and water vapor in the atmosphere. It assumes a constant wind speed and models cooler rural air as it is advected over an urban area that has a different surface energy budget due to the difference in the thermal and hydrological surface properties. These urban surface properties reduce their ability to store surface water and increase their ability to store thermal energy. The advected air is thus heated over the city by the increased sensible heat flux [term H in Eq. (1)], which results in an urban thermal boundary layer (as conceptually depicted in Fig. 1). The final equations and findings of the model are reported in a later section, the full details and derivations are included in the appendix, and MATLAB code is provided online in the supplementary material of the paper.

3. Results

In this section, we examine the difference between urban and rural temperatures (i.e., the urban heat island effect) using observational datasets, the WRF model, and the analytical model.

a. Observational analyses

The 2-m air temperatures measured at DMH in downtown Baltimore and at BWI in the suburbs of Baltimore are presented in Fig. 3. Here, we primarily examine the differences in the daytime- and nighttime-averaged air temperatures between the DMH and BWI sites, which represent the urban heat island effect and are shown in the bottom panel of Fig. 5. The top panel of Fig. 5 is a direct comparison between the 2-m air temperatures at DMH and BWI (reproduced from Fig. 3). As can be seen from Fig. 5, the heat wave event lasts from 7 to 10 June: the maximum daytime air temperatures at the urban and suburban/rural sites are 5°–10°C larger during the heat wave period than before or after. The large-scale weather conditions for the heat wave event indicate that it was primarily caused by a stagnant high pressure system that is centered over Georgia and South Carolina during 7–10 June 2008 (not shown). The impacts of the heat wave conditions extend farther north and significantly affect the Baltimore area.

The trends in the bottom panel of Fig. 5 illustrate that, during the heat wave period, the daytime and nighttime UHI indices are both enhanced significantly compared to the period before the heat wave, implying synergistic interactions between the urban heat island and the heat wave. The urban heat island effect at night is invariably larger than its daytime counterpart, which is consistent with previous observational (Oke 1982) and modeling studies (Oleson et al. 2011; Fischer et al. 2012). This is due to larger daytime heat storage in urban areas than in rural areas (the WRF simulations discussed next

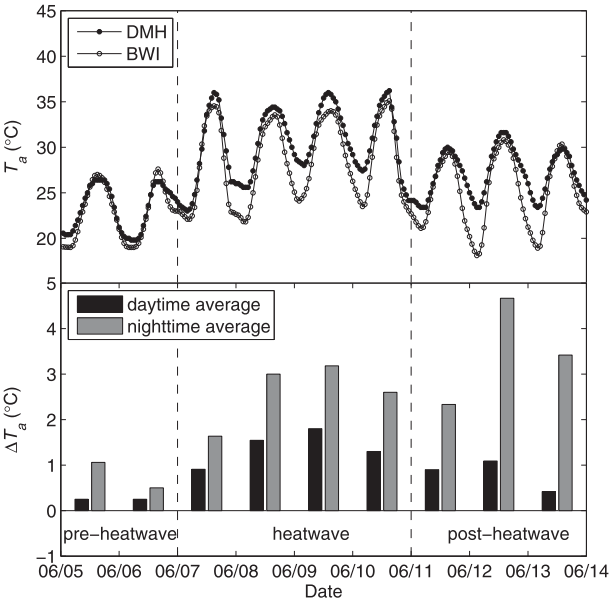

FIG. 5. (top) The 2-m air temperatures measured at DMH and at BWI in Baltimore MD. (bottom) The difference between the urban and rural air temperatures, i.e., the UHI index ΔT_a, for daytime and nighttime. The heat wave event lasts from 7 to 10 Jun.

indicate that the daily averaged ground heat flux term in urban terrain exceeded its rural counterpart by about $5\,\mathrm{W\,m^{-2}}$); this stored heat is subsequently released during nighttime (Oke 1982; Oleson et al. 2011; Fischer et al. 2012). This higher heat storage capacity in urban areas is also the cause of the lag in the peak of the nighttime temperature difference, which occurs after the heat wave period on 12 June. Inspection of the air temperatures at the two sites (Fig. 5, top) reveals that, after the heat wave period, the nighttime temperature in rural areas drops more rapidly and substantially than in the urban areas, which continue to be heated by the energy stored in the ground.

b. Spatially averaged numerical analyses

A broader and more spatially representative comparison was then conducted using high-resolution numerical simulations with WRF, where air/surface temperature contrasts between urban and rural areas are quantified. The daily, daytime-, and nighttime-averaged 2-m air temperature differences between the urban (spatially averaged over all urban grid cells in Baltimore; see Fig. 2) and rural (spatially averaged over all rural grid cells in Baltimore; see Fig. 2) areas are presented in Fig. 6. The contrasts in the 2-m air temperature between urban and rural areas evidently confirm that the UHI is amplified during the heat wave period relative to the preceding and following periods. The 2-m air temperature comparison

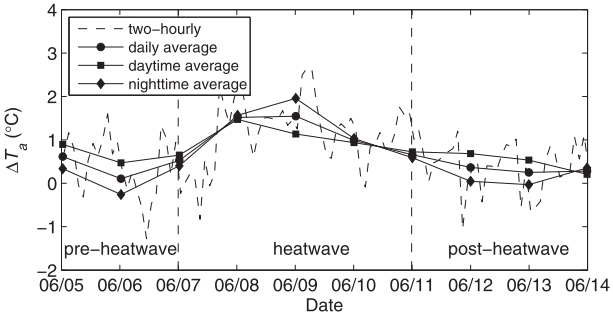

FIG. 6. The 2-m air temperature differences between the urban and rural areas around Baltimore simulated by WRF. The temperature differences are boosted during the heat wave period.

also indicates that the nighttime UHI during the heat wave period is slightly stronger than the daytime UHI. The spatially averaged simulation results are hence in good qualitative agreement with the single-point observations in Fig. 5, despite the significant differences in their characteristic spatial scales. Nonetheless, some differences are also seen between spatially averaged numerical analyses and single-point observational analyses. For example, in the spatially averaged numerical analyses, the daytime UHI is slightly stronger than the nighttime UHI preceding and following the heat wave period.

The spatially averaged surface temperatures simulated by WRF are shown in the top panel of Fig. 7 and the urban–rural differences are shown in the bottom panel. The UHI effect based on surface temperature is fairly constant before the heat wave period and starts to increase as the heat wave begins. It reaches its maximum shortly after the event rather than during the heat wave period. This phase shift in the peak UHI index based on surface temperature is again a signature of the larger heat storage in the urban canopy and ground than in the rural areas. Figure 8 shows the urban (G_u) and rural (G_r) ground heat fluxes and the daily averaged urban–rural ground heat flux differences ($\Delta G = G_u - G_r$). As can be seen from Fig. 8, the ground heat flux in urban areas has a much larger diurnal cycle due to the large heat storage capacity of urban areas. Before 10 June, the daily averaged ground heat flux differences are always positive, implying that urban areas are storing more heat than the rural areas; this results in a larger urban surface temperature as well as a continuously increasing surface temperature-based UHI index. Toward the end of the heat wave event, the daily averaged ground heat flux differences are close to zero, indicating that urban areas and rural areas store the same amount the heat and hence the UHI index is maintained constant. By 13 and 14 June, the daily averaged ground heat flux difference becomes negative and the UHI index starts to decrease.

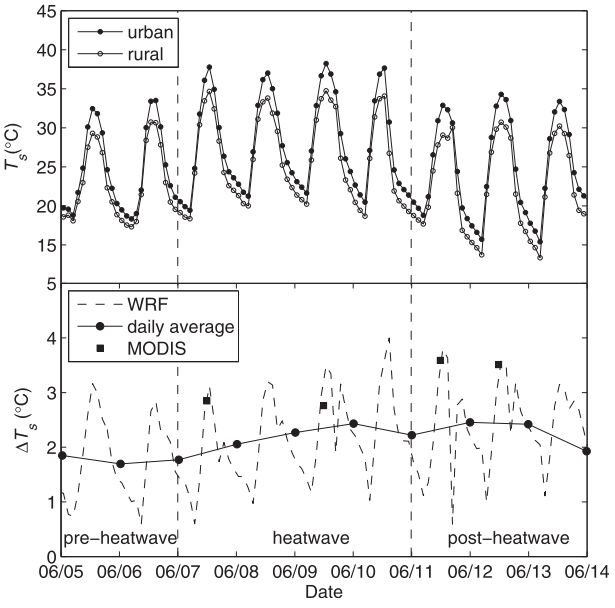

FIG. 7. (top) Urban and rural surface temperatures around Baltimore simulated by WRF. (bottom) Urban and rural surface temperature differences (ΔT_s) simulated by WRF and measured by MODIS.

The negative daily averaged ground heat flux difference on 10 June is responsible for a slight decrease in the UHI index observed on 11 June. This lag in ΔG drives and explains the lag (phase shift) in the surface temperature-based UHI index.

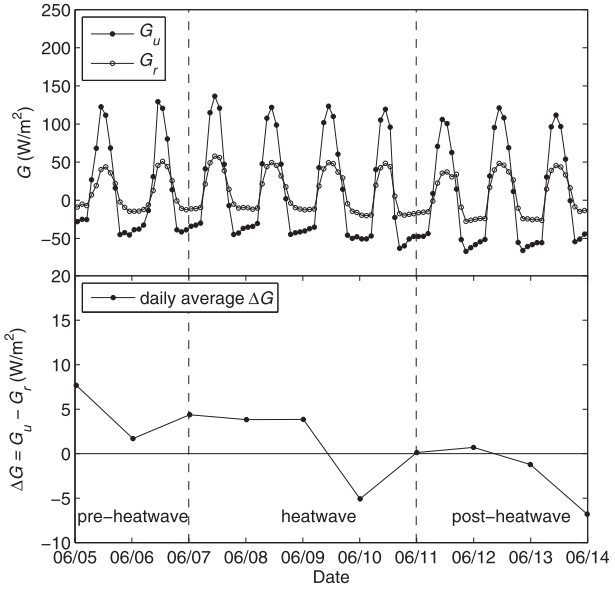

FIG. 8. (top) Urban (G_u) and rural (G_r) ground heat fluxes around Baltimore simulated by WRF. (bottom) Daily averaged urban–rural ground heat fluxes differences (ΔG) simulated by WRF.

To corroborate these findings based on WRF, satellite-measured land surface temperatures from MODIS on 7, 9, 11, and 12 June are also used. The same criterion is applied for MODIS-observed land surface temperature to separate urban surface temperature from rural temperature and the same averaging procedure is employed. As confirmed by the black squares in the bottom panel of Fig. 7, the post–heat wave period (11 and 12 June) has a larger surface temperature difference between urban areas and rural areas compared to the heat wave period (7 and 9 June). The increase in the UHI index based on surface temperature simulated by WRF is in very good agreement with the one measured by MODIS, which is consistent with our validation results (Fig. 4). We should stress, however, that the simulated urban and rural surface (and air) temperatures reach their maxima during the heat wave period and this period remains the riskiest for human health. It is the difference between urban and rural surface temperatures that reaches its maximum toward the end of or slightly after the heat wave period due to high heat storage in urban terrain. This heat storage is a serious adverse effect since it can potentially extend extreme heat conditions in urban areas, which as presented earlier in the paper increases the mortality risk by 0.38% for each additional heat wave day.

c. An analytical model

The measurements and modeling results presented so far point to a significant exacerbation in thermal comfort conditions in cities during heat waves, exceeding the linearly combined deterioration resulting from separate heat waves and urban heat islands. This indicates that, in a warming future climate, the urban population (especially the most vulnerable groups such as the elderly and the poor who have no access to air conditioning) will be at a great risk of heat-related mortality and morbidity. But an open question remains as to whether these findings are unique to Baltimore and to this heat wave, or are more general. A related question concerns the physical processes that are driving this synergistic interaction, which, if elucidated, can help in designing mitigation strategies. To address these questions, we develop a simple analytical model that includes the main physical processes that can contribute to the synergistic interaction observed and simulated between UHIs and HWs.

As introduced before, the model solves simultaneously for the heat and water vapor transfer between an urban surface and the atmosphere, coupled with the vertical turbulent transport and horizontal mean advection of heat and water vapor in the air following the approach of Yeh and Brutsaert (1971a,b). The urban temperatures are calculated given the conditions over upwind rural areas (including rural surface temperature and surface moisture availability), the prevailing wind speed, and the urban surface properties. The final expression of the model, whose development is detailed in the appendix, yields the following representation for the UHI index ΔT:

$$\mathrm{UHI} = T_u(x,z) - T_r(z) = (1-\beta_u/\beta_r)T^*_{\mathrm{rs}} f_1(x,z) + g(u_{10})(Q_u - Q_r) f_2(x,z), \quad (2)$$

where $T_u(x, z)$ is the urban temperature (K) as a function of the along-wind direction x and the vertical direction z ($0 < x < x_u$ is the urban area; $x < 0$ and $x > x_u$ is the rural area; $z = 0$ is the surface); T_r is the upwind rural temperature (K), which is only a function of height z; and β_u and β_r are the ratios of actual surface specific humidities divided by the saturated surface specific humidities for the urban and rural surfaces (at the corresponding surface temperatures following the Clausius–Clapeyron relation), respectively. These ratios range from 0 to 1 and represent the moisture availability of urban and rural surfaces, a value of 1 indicating a wet surface. In Eq. (2), $T^*_{\mathrm{rs}} = q_{\mathrm{rs}}/(c_p/L_v + \alpha\beta_u)$, where q_{rs} is the actual rural (background) surface specific humidity ($\mathrm{kg\,kg^{-1}}$), c_p is the specific heat capacity of air at constant pressure ($\mathrm{J\,kg^{-1}\,K^{-1}}$), L_v is the latent heat of vaporization of water ($\mathrm{J\,kg^{-1}}$), and α is the derivative of the saturated specific humidity with respect to temperature at $T = T_{\mathrm{rs}}$. The quantity $g(u_{10})$ is a positive function that depends on, and decreases with, the mean wind speed at the reference level of 10 m, u_{10} ($\mathrm{m\,s^{-1}}$); $Q_u - Q_r$ is the difference in available energy ($Q = R_n - G$) between urban and rural areas; and $f_1(x, z)$ and $f_2(x, z)$ are functions that are only dependent on locations x and z and that come from the coupled solution of the advection–diffusion equations describing this problem. Full details about the derivation of this model are included in the appendix.

From Eq. (2), one can note that the UHI index has two primary determinants: the first comes from the moisture availability ratio between the urban (β_u) and rural (β_r) areas [first term in Eq. (2)]; the second comes from a combination of wind speed effects through $g(u_{10})$ and the available energy difference between the urban and rural areas ($Q_u - Q_r$) [second term in Eq. (2)]. With this model, the role and magnitude of the three possible interactions between HWs and UHIs described in the introduction can be unraveled. The model yields the UHI index as a function of height and horizontal location and can predict the changes in UHI intensity for slightly strengthened local wind speeds due to

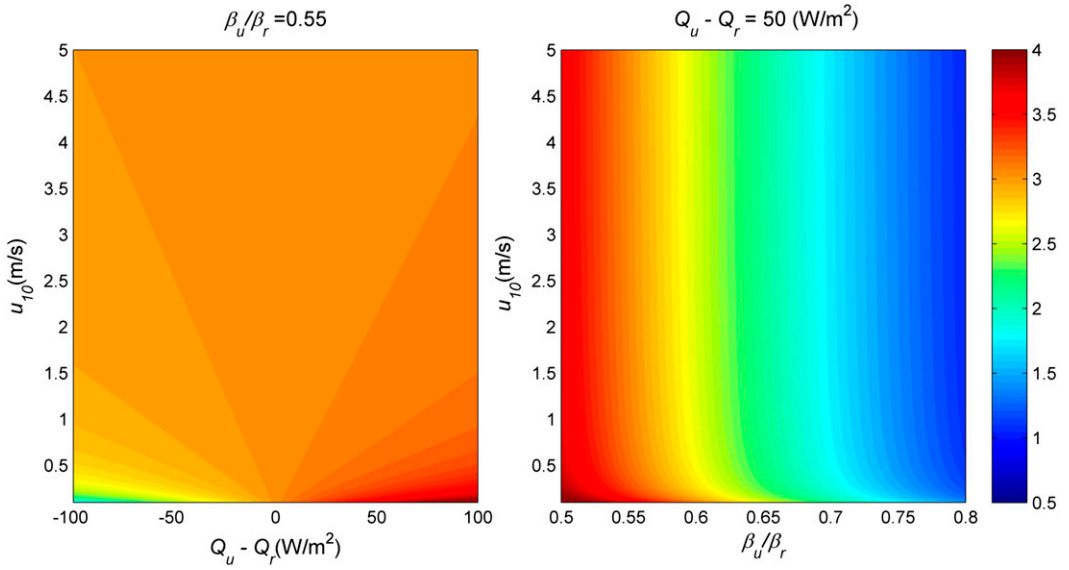

FIG. 9. Averaged air temperature differences (°C) at 2 m between urban and rural areas as functions of the wind speed (u_{10}) and (right) the moisture availability difference (β_u/β_r), and (left) the available energy difference ($Q_u - Q_r$), produced by the analytical model [Eq. (2)] over an urban surface 10 km in length, representing Baltimore. Detailed model inputs are discussed in the appendix.

secondary circulations, lower regional wind speeds during heat wave periods, and various differences in surface water availability. The effects of differences in urban and rural albedos can also be investigated through the available energy difference ($Q_u - Q_r$).

The dependence of the UHI index, for 2-m air temperature averaged over a 10-km urban patch representing a midsize city comparable to Baltimore, on the moisture availability difference (β_u/β_r), the wind speed (u_{10}), and the available energy difference ($Q_u - Q_r$) is illustrated in Fig. 9. One can note the following:

1) The UHI index is positively correlated with the available energy difference ($Q_u - Q_r$), as can be seen from the left panel of Fig. 9. Typical values of the difference in available energy between the urban and rural surfaces ($Q_u - Q_r$) were obtained from WRF and they range from -100 to 100 W m^{-2}. Positive available energy differences usually occur during the nighttime when the urban surface is releasing all the heat stored during the day and evapotranspiration is close to zero over both urban and rural surfaces. This is consistent with many previous studies that describe the UHI as mainly a nighttime phenomenon (Oke 1982; Oleson et al. 2011; Fischer et al. 2012). During the day, and despite a negative energy difference (more available energy over rural terrain), the UHI index remains positive due to the energy partitioning that results in higher sensible heat fluxes H (and lower latent heat fluxes) over the dry urban area.
2) The wind speed impact on the urban heat island effect is dependent on the available energy difference $Q_u - Q_r$, as illustrated in the left panel of Fig. 9. When the available energy difference ($Q_u - Q_r$) is negative (usually occurs during daytime when the urban areas are storing a lot of energy and G_u is high), the air temperature difference increases with increasing wind speed. In this case, the wind speed effect here is mainly to increase the urban-atmosphere energy exchanges; therefore, increasing wind speed exacerbates the UHI effect. When the available energy difference ($Q_u - Q_r$) is positive, during the nighttime, the air temperature difference increases with decreasing wind speed, as can be seen in both panels of Fig. 9. Reduced advective cooling is the dominant effect of reduced wind speeds in this case. Consequently, the lower wind speed associated with heat waves is particularly detrimental to the urban microclimatology at night when it acts as a synergistic factor that also exacerbates the urban heat island effect.
3) Because of the moisture limitation in urban areas, β_u will be generally smaller than β_r. It can be seen from the right panel of Fig. 9 that smaller β_u/β_r ratios favor more intense UHIs in urban areas. Furthermore, as the temperature increases (i.e., as the heat wave sets in), the saturated surface specific humidities (which are nonlinear functions of surface temperatures) will increase over both urban and rural areas. The actual specific humidity over the urban area will be moisture

limited due to the dry impervious surfaces and the spatially averaged β_u will decrease significantly, while the actual specific humidity over the wetter rural area will be able to rise with the rising saturated value (thus favoring evaporation and acting as a negative feedback to the rising temperatures over rural terrain) and β_r will remain unchanged or increase slightly [see theoretical and observational results of Bateni and Entekhabi (2012)]. Consequently, β_u/β_r will decrease and the UHI effect will be exacerbated during heat waves. A reasonable indicator for moisture limitation in urban areas, relative to rural areas, is the impervious surface fraction, assuming that vegetated urban areas behave like rural ones while impervious surfaces hold no moisture. The impervious surface fraction of Baltimore calculated from WRF is 0.55 (used as the baseline value for β_u/β_r in the left panel of Fig. 9). As can be seen from the right panel in Fig. 9, when the moisture availability in urban areas is low (e.g., when $\beta_u/\beta_r < 0.7$), the effects of wind speed are diminished and the UHI index is dominated by β_u/β_r. Comparing the different effects (i.e., the moisture availability difference, available energy difference, and the wind speed effect) reveals that the UHI is most sensitive to the moisture availability difference, which always acts as a synergistic interaction factor between urban heat islands and heat waves. This is in qualitative agreement with the results of Fischer et al. (2007), who observe, using climate simulations, that the limitation of evaporation is the major factor that amplifies temperature extremes and increases the number of hot days over Europe during four recent heat waves.

This analytical model is designed to more fundamentally explain the interactions between urban heat islands and heat waves without invoking high-resolution numerical simulations or observational datasets. It captures the key physical processes that are responsible for the synergies between the two phenomena, namely, the moisture and energy availability differences and the wind speed effect.

4. Conclusions and discussion

In this study, the interactions between urban heat islands and heat waves are investigated using a combination of observational, numerical, and analytical analyses. The urban heat island effect as defined on the basis of 2-m air temperature and surface temperature during a heat wave event (7–10 June 2008) over the Baltimore area is quantified. Both observations and WRF simulations indicate that the urban heat island effect is amplified during the heat wave period. An analytical model is then developed to unravel the physical mechanisms that are responsible for the interactions between urban heat islands and heat waves. The model results indicate that the shift of the surface energy partitioning toward higher evaporation is a significant mitigation mechanism during heat waves in rural areas [as in Bateni and Entekhabi (2012)], but it is hindered in urban areas by the lack of vegetation and surface moisture. This largely explains the increase in UHI indices during heat waves. Other factors such as the decreasing wind speed during heat wave conditions also contribute to the synergistic interactions.

The most striking general finding of this study is that, not only do heat waves increase the absolute magnitudes of urban and rural temperatures, but more critically, they synergistically interact with urban heat islands to intensify the difference between the urban and rural temperatures and thus result in higher heat-related impacts in cities. Considering the rural area as a reference, urban populations are already living in a hotter environment due to the urban heat island effect. The synergistic interactions between heat waves and urban heat islands exacerbate the hostile micrometeorological conditions in cities.

Urban areas are emerging as the nexus of the energy, water, health, and climate challenges facing humanity in this century and beyond. This study illustrates these intersecting challenges and raises some significant concerns about the ability of current cities to deal with future risks. With the predicted intensification and lengthening of heat waves under a changing climate, city residents will be at a significantly higher health risk than their rural counterparts. With increasing urban populations and extreme heat events, the stress on electric grids designed for lower loads is also going to increase significantly. Blackouts during heat waves can be especially devastating given the reliance of a large fraction of the population on air conditioning during such events. Adaptation and mitigation strategies, such as green/cool roofs and green spaces, are therefore critically needed in order to reduce the adverse health and other impacts related to the heat stress induced by interacting urban heat islands and heat waves. Vegetation restores moisture availability in urban areas and reactivates the negative feedback on urban temperatures associated with evaporation. White roofs and reflective pavements reduce the available energy in urban areas and thus can also help alleviate the urban heat island effect.

The limitations of this study that are important to appreciate are related to the observational analysis that is mainly based on measurements from two sites and to the simulation of a single heat wave event. While the analytical model aims to generalize the findings by unraveling the physical mechanisms dominating UHI strength

during heat waves, future work involving more observational datasets and considering more HW events to confirm these synergistic interactions would be valuable. The analytical model can also be further improved to explicitly represent heat storage and release in urban and rural surfaces (thus requiring only incoming long- and shortwave radiation as inputs) and to include urban anthropogenic heat releases without compromising the analytical nature of the model. With such improvements, the model would become a general UHI model that would be valuable even during periods without heat waves.

Acknowledgments. This study was funded by the National Science Foundation under Grant CBET-1058027. The authors thank James A. Smith, Mary-Lynn Baeck, and Maofeng Liu from Princeton University and Ting Sun from Tsinghua University for their help, particularly in obtaining and processing some of the observational datasets. The authors also thank the three reviewers whose comments helped improve the paper considerably.

APPENDIX

Analytical Model Description and Setup

The model we develop here is based on a previously proposed analytical model that simultaneously solves for the turbulent heat and water vapor transfer between a surface of limited extent and the atmosphere (Yeh and Brutsaert 1971a). The original model considers a limited water surface, but here we modify it for application to a limited urban surface. The revised model examines the urban surface heat and water vapor exchanges with the atmosphere by coupling the surface energy budget with simplified equations for thermal energy and water vapor transport in the atmosphere. The urban surface–air temperatures and specific humidities are hence calculated given the upwind conditions over rural areas, including rural surface temperature and surface moisture availability, the prevailing wind speed, and the urban surface properties. MATLAB code for this analytical model is provided online in the supplementary material to this paper (http://dx.doi.org/10.1175/JAMC-D-13-02.s1).

The analytical model considers a two-dimensional domain (with a streamwise coordinate x and a vertical coordinate z) and a sudden change in the surface moisture and temperature conditions at $x = 0$. By assuming stationarity and ignoring differences in the wind speed between the urban and rural surfaces due to potential changes in surface roughness, the governing conservation equations for heat and water vapor can be reduced to two simple advection–diffusion equations:

$$\overline{u}\frac{\partial \overline{T}}{\partial x} = -\frac{\partial \overline{w'T'}}{\partial z} \quad \text{and} \tag{A1}$$

$$\overline{u}\frac{\partial \overline{q}}{\partial x} = -\frac{\partial \overline{w'q'}}{\partial z}, \tag{A2}$$

where u is the streamwise (x direction) velocity, w is the vertical (z direction) velocity, T is the temperature, and q is the specific humidity. The overbars indicate the Reynolds averages and the primes indicate turbulent excursions from the Reynolds averages (Stull 1988). Invoking a first-order closure model for the turbulent fluxes $\overline{w'T'}$ and $\overline{w'q'}$ yields

$$\overline{u}\frac{\partial \overline{T}}{\partial x} = \frac{\partial}{\partial z}\left(K_h\frac{\partial \overline{T}}{\partial z}\right) \quad \text{and} \tag{A3}$$

$$\overline{u}\frac{\partial \overline{q}}{\partial x} = \frac{\partial}{\partial z}\left(K_q\frac{\partial \overline{q}}{\partial z}\right), \tag{A4}$$

where K_h and K_q are turbulent diffusivities for temperature and water vapor, respectively (Stull 1988). Furthermore, it is assumed that temperature and water vapor are transported by turbulence with the same efficiency (Li and Bou-Zeid 2011; Li et al. 2012), which varies with height above the surface following a power law $K_h = K_q = K = bz^n$. The mean wind profile also follows a power law:

$$\overline{u} = az^m, \tag{A5}$$

where n and m are constants, for which the values $m = 1/7$ and $n = 1 - m = 6/7$ are used (Brutsaert 1982; Stull 1988). On the other hand, a and b are formulated as functions of the surface shear stress (represented by the friction velocity u_*) and the surface roughness length z_0 following $a = 5.5u_*/z_0^m$ and $b = 5u_*z_0^m/5.5\,\text{m}$ (Yeh and Brutsaert 1971b). Following Stull (1988), u_* can be calculated from the log law via $u_* = \kappa u_{10}/\log(10/z_0)$, where u_{10} is the mean wind speed at the reference height of 10 m. Usually, z_0 is linked to the urban canopy height (e.g., Bou-Zeid et al. 2009) and is given the representative value of 1.25 m in this study. Given a value of z_0, a and b only vary with the friction velocity u_*, and thus with u_{10}.

The boundary conditions for Eqs. (A1)–(A5) are as follow.

1) When $x < 0$, the surface is rural (indicated by the subscript r):

$$\begin{cases} \overline{T}_r = T_{\rm rs}; \quad \overline{q}_r = q_{\rm rs} = \beta_r q^*(T_{\rm rs}) & \\ R_{\rm nr} = H_r + {\rm LE}_r + G_r = -c_p \rho K \dfrac{\partial \overline{T}_r}{\partial z} - L_v \rho K \dfrac{\partial \overline{q}_r}{\partial z} + G_r & z = 0, \quad x < 0, \end{cases} \tag{A6}$$

where $T_{\rm rs}$ and $q_{\rm rs}$ are the surface temperature and the surface specific humidity at the rural surface, respectively, and q^* is the saturated specific humidity and thus is only a function of temperature. The ratio of the surface specific humidity to the saturated one ($q_{\rm rs}/q^*$) represents the moisture availability at the surface, which is denoted by the β_r parameter here. The net radiation over the rural surface is $R_{\rm nr} = ({\rm SW_{in}} - {\rm SW_{out}} + {\rm LW_{in}} - {\rm LW_{out}})_r$. It arises from the radiative balance between the incoming shortwave radiation ($\rm SW_{in}$), the outgoing shortwave radiation ($\rm SW_{out}$), the incoming longwave radiation ($\rm LW_{in}$), and the outgoing longwave radiation ($\rm LW_{out}$). As mentioned in the main text, the net radiation is partitioned into three parts: the sensible heat flux H, the latent heat flux (LE), and the ground heat flux G. The sensible and latent heat fluxes are related to the vertical gradients of air temperature and specific humidity via the turbulent diffusivity K, while ρ is the air density ($=1.2\,{\rm kg\,m^{-3}}$), c_p is the specific heat capacity of air at constant pressure ($\rm J\,kg^{-1}\,K^{-1}$), and L_v is the latent heat of vaporization of water ($\rm J\,kg^{-1}$).

2) When $0 < x < x_u$, the surface is urban (indicated by the subscript u), where x_u is the size of the urban patch. The boundary conditions for the urban zone are then specified as

$$\begin{cases} \overline{T} = \overline{T}_r(z); \quad \overline{q} = \overline{q}_r(z) & z > 0, \quad x = 0 \\ \overline{T} = T_{\rm us}; \quad \overline{q} = q_{\rm us} = \beta_u q^*(T_{\rm us}) & z = 0, \quad 0 < x < x_u \\ R_{\rm nu} = H_u + {\rm LE}_u + G_u = -c_p \rho K \dfrac{\partial \overline{T}}{\partial z} - L_v \rho K \dfrac{\partial \overline{q}}{\partial z} + G_u & z = 0, \quad 0 < x < x_u \end{cases}, \tag{A7}$$

where T_r and q_r are the rural air temperature and the rural air specific humidity, which are assumed to be only functions of z (i.e., the incoming flow is in equilibrium with the upstream rural surface conditions). Similarly, $T_{\rm us}$ and $q_{\rm us}$ are the surface temperature and the surface specific humidity at the urban surface, respectively, and β_u indicates the moisture availability in the urban areas. The net radiation over the urban surface is $R_{\rm nu} = ({\rm SW_{in}} - {\rm SW_{out}} + {\rm LW_{in}} - {\rm LW_{out}})_u$.

3) When $x > x_u$, the surface becomes rural again (this would allow the investigation of the downwind impact of urban areas, but we do not elaborate on this impact in this study):

$$-c_p \rho K \frac{\partial \overline{T}}{\partial z} = H_r \quad \text{and} \quad -L_v \rho K \frac{\partial \overline{q}}{\partial z} = {\rm LE}_r \qquad z = 0, \quad x > x_u. \tag{A8}$$

After introducing the following dimensionless variables,

$$\theta = \frac{T - T_r}{T_m - T_{\rm rs}}, \quad \chi = \frac{q - q_r}{q_m - q_{\rm rs}}, \tag{A9}$$

$$\xi = x/x_u, \quad \text{and} \quad \zeta = \left(\frac{a}{b x_u}\right)^{\nu} \frac{z^{1-n}}{(1-n)^{2\nu}}, \tag{A10}$$

where $\nu = (1-n)/(2+m-n)$ is a constant since it is determined by m and n that we take as constants, the representative temperature and specific humidity scales for urban areas are T_m and q_m, which will cancel out later in the derivations and are thus not important. The overbars are omitted for simplicity and the governing equations become

$$\frac{\partial^2 \chi}{\partial \zeta^2} - \zeta^{(1-2\nu)/\nu} \frac{\partial \chi}{\partial \xi} = 0 \quad \text{and} \quad \frac{\partial^2 \theta}{\partial \zeta^2} - \zeta^{(1-2\nu)/\nu} \frac{\partial \theta}{\partial \xi} = 0. \tag{A11}$$

The boundary conditions become

$$\begin{cases} \theta = 0; \quad \chi = 0 & \zeta > 0, \quad \xi = 0 \\ c_1 \dfrac{\partial \theta}{\partial \zeta} + c_2 \dfrac{\partial \chi}{\partial \zeta} + c_3 = 0 & \zeta = 0, \quad 0 < \xi < 1 \\ \chi = c_4 \theta + c_5 & \zeta = 0, \quad 0 < \xi < 1 \\ \dfrac{\partial \theta}{\partial \zeta} = 0; \quad \dfrac{\partial \chi}{\partial \zeta} = 0 & \zeta = 0, \quad \xi > 1 \end{cases}, \tag{A12}$$

where the coefficients are

$$c_1 = c_p \rho b \left(\frac{a}{b x_u}\right)^{\nu} (1-n)^{1-2\nu} (T_m - T_{\rm rs}),$$

$$c_2 = L_v \rho b \left(\frac{a}{b x_u}\right)^{\nu} (1-n)^{1-2\nu} (q_m - q_{\rm rs}),$$

$$c_3 = R_{\rm nu} - R_{\rm nr} - (G_u - G_r) = (R_{\rm nu} - G_u) - (R_{\rm nr} - G_r) = Q_u - Q_r,$$

$$c_4 = \beta_u \frac{(T_m - T_{\rm rs})}{(q_m - q_{\rm rs})} \frac{dq^*}{dT}\bigg|_{T=T_{\rm rs}} = \beta_u \frac{(T_m - T_{\rm rs})}{(q_m - q_{\rm rs})} \alpha, \quad \text{and}$$

$$c_5 = \frac{(\beta_u q^*_{\rm rs} - q_{\rm rs})}{(q_m - q_{\rm rs})} = \frac{(\beta_u/\beta_r - 1) q_{\rm rs}}{(q_m - q_{\rm rs})}, \tag{A13}$$

where $\alpha = (dq^*/dT)|_{T=T_{\rm rs}}$ is the derivative of the saturated specific humidity with respect to air temperature and is taken here as a constant ($=1.87 \times 10^{-3}\,{\rm K}^{-1}$) given the limited temperature range of interest (Brutsaert 2005). The available energy is Q ($=R_n - G$), which according to the surface energy balance is equal to the sum of the sensible and latent heat fluxes. The difference in the available energy between urban and rural areas is $Q_u - Q_r$, which is assumed to be constant in the derivations.

Solving Eq. (A11) with the boundary conditions specified in Eqs. (A12) and (A13) yields the urban temperature and specific humidity (Yeh and Brutsaert 1971a):

$$\frac{T - T_r}{T_m - T_{\rm rs}} = -\frac{c_2 c_5}{c_1 + c_2 c_4} \frac{\Gamma(\nu, \eta)}{\Gamma(\nu)} + \frac{c_3}{c_1 + c_2 c_4} \frac{\nu^{1-2\nu}}{\Gamma(1-\nu)} \times \xi^{\nu} \eta^{(\nu-1)/2} e^{-\eta} W_{-(1+\nu)/2,\nu/2}(-\eta) \quad \text{and} \tag{A14}$$

$$\frac{q - q_r}{q_m - q_{\rm rs}} = \frac{c_1 c_5}{c_1 + c_2 c_4} \frac{\Gamma(\nu, \eta)}{\Gamma(\nu)} + \frac{\alpha \beta_u c_3}{c_1 + c_2 c_4} \frac{\nu^{1-2\nu}}{\Gamma(1-\nu)} \times \xi^{\nu} \eta^{(\nu-1)/2} e^{-\eta} W_{-(1+\nu)/2,\nu/2}(-\eta), \tag{A15}$$

where $\eta = \nu^2 \xi^{1/\nu}/\xi$ and is only dependent on x and z, Γ is the gamma function (the incomplete gamma function when it involves two arguments), and W is the Whittaker function. Substituting c_1, c_2, c_3, and c_4 into Eqs. (A14) and (A15) yields

$$T - T_r = (1 - \beta_u/\beta_r) T^*_{\rm rs} f_1(x,z) + g(u_{10})(Q_u - Q_r) f_2(x,z) \tag{A16}$$

and

$$q - q_r = -(1 - \beta_u/\beta_r) q^*_{\rm rs} f_1(x,z) + \alpha \beta_u g(u_{10})(Q_u - Q_r) f_2(x,z), \tag{A17}$$

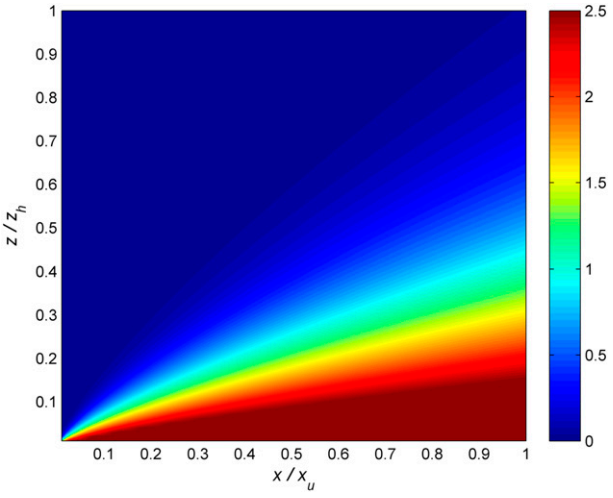

FIG. A1. The growth of the urban thermal boundary layer over an urban patch with $x_u = 10\,{\rm km}$, $z_h = 1\,{\rm km}$, $u_{10} = 3\,{\rm m\,s^{-1}}$, $\beta_u/\beta_r = 0.78$, and $Q_u - Q_r = 50\,{\rm W\,m^{-2}}$.

where $T^*_{\rm rs} = q_{\rm rs}/(c_p/L_v + \alpha\beta_u)$ and $q^*_{\rm rs} = q_{\rm rs}/(1 + \alpha\beta_u L_v/c_p)$. The quantity $g(u_{10})$ is a positive function that decreases with u_{10}:

$$g(u_{10}) = \frac{1}{\rho(c_p + \alpha\beta_u L_v)} \frac{a^{\nu}}{b^{\nu-1}} (1-n)^{1-2\nu} \frac{\nu^{1-2\nu}}{\Gamma(1-\nu)}. \tag{A18}$$

Note that n and ν are both constants and will not change with heat wave conditions and thus $g(u_{10})$ depends only on a (which depends on u_{10}) and b (which depends on the turbulent diffusivity that in this model is also directly related to u_{10}). The functions $f_1(x, z)$ and $f_2(x, z)$ are only dependent on locations x and z:

$$f_1(x,z) = \Gamma(\nu, \eta)/\Gamma(\nu) \quad \text{and} \tag{A19}$$

$$f_2(x,z) = x^{\nu} \eta^{(\nu-1)/2} e^{-\eta} W_{-(1+\nu)/2,\nu/2}(-\eta). \tag{A20}$$

As can be seen from Eq. (A16), the difference between the urban and rural temperatures depends on u_{10}, β_u/β_r, and $Q_u - Q_r$. In this study, the size of the urban patch x_u is assumed to be 10 km, representing Baltimore. The value of $q_{\rm rs}$ is chosen to be $0.010\,{\rm kg\,kg^{-1}}$ and β_r is set to be 0.9. By varying u_{10}, β_u/β_r, and the available energy differences based on Eq. (A16), the sensitivities of the urban heat island effect to the prevailing wind speed, the moisture availabilities, and the available energy differences are explored. Figure A1 shows a particular case in which the values of u_{10}, β_u/β_r, and the available energy difference are taken as $3\,{\rm m\,s^{-1}}$, $0.78\,{\rm W\,m^{-2}}$, and $50\,{\rm W\,m^{-2}}$, respectively. It can be seen that a thermal boundary layer with hotter air temperatures develops over the urban patch, consistently with the conceptual depiction in Fig. 1.

REFERENCES

Ackerman, S. A., and J. Knox, 2012: *Meteorology: Understanding the Atmosphere.* 3rd ed. Jones and Bartlett Learning, 578 pp.

Anderson, G. B., and M. L. Bell, 2011: Heat waves in the United States: Mortality risk during heat waves and effect modification by heat wave characteristics in 43 U.S. communities. *Environ. Health Perspect.,* **119,** 210–218.

Basara, J. B., H. G. Basara, B. G. Illston, and K. C. Crawford, 2010: The impact of the urban heat island during an intense heat wave in Oklahoma City. *Adv. Meteor.,* **2010,** 230365, doi:10.1155/2010/230365.

Bateni, S. M., and D. Entekhabi, 2012: Relative efficiency of land surface energy balance components. *Water Resour. Res.,* **48,** doi:10.1029/2011WR011357.

Bou-Zeid, E., J. Overney, B. D. Rogers, and M. B. Parlange, 2009: The effects of building representation and clustering in large-eddy simulations of flows in urban canopies. *Bound.-Layer Meteor.,* **132,** 415–436.

Brutsaert, W., 1982: *Evaporation into the Atmosphere: Theory, History, and Applications.* Reidel, 299 pp.

——, 2005: *Hydrology: An Introduction.* Cambridge University Press, 605 pp.

Chen, F., and Coauthors, 2011: The integrated WRF/urban modelling system: Development, evaluation, and applications to urban environmental problems. *Int. J. Climatol.,* **31,** 273–288.

Fischer, E. M., S. I. Seneviratne, D. Luthi, and C. Schar, 2007: Contribution of land-atmosphere coupling to recent European summer heat waves. *Geophys. Res. Lett.,* **34,** L06707, doi:10.1029/2006GL029068.

——, K. W. Oleson, and D. M. Lawrence, 2012: Contrasting urban and rural heat stress responses to climate change. *Geophys. Res. Lett.,* **39,** L03705, doi:10.1029/2011GL050576.

Fry, J., and Coauthors, 2011: Completion of the 2006 National Land Cover Database for the conterminous United States. *Photogramm. Eng. Remote Sens.,* **77,** 858–864.

Grimm, N. B., S. H. Faeth, N. E. Golubiewski, C. L. Redman, J. G. Wu, X. M. Bai, and J. M. Briggs, 2008: Global change and the ecology of cities. *Science,* **319,** 756–760.

Grimmond, C. S. B., 2007: Urbanization and global environmental change: Local effects of urban warming. *Geogr. J.,* **173,** 83–88.

——, and Coauthors, 2010: The International Urban Energy Balance Models Comparison Project: First results from phase 1. *J. Appl. Meteor. Climatol.,* **49,** 1268–1292.

——, and Coauthors, 2011: Initial results from phase 2 of the International Urban Energy Balance Model Comparison. *Int. J. Climatol.,* **31,** 244–272.

Hidalgo, J., V. Masson, and L. Gimeno, 2010: Scaling the daytime urban heat island and urban-breeze circulation. *J. Appl. Meteor. Climatol.,* **49,** 889–901.

Lebassi, B., and Coauthors, 2009: Observed 1970–2005 cooling of summer daytime temperatures in coastal California. *J. Climate,* **22,** 3558–3573.

——, J. Gonzalez, and R. Bornstein, 2011: Modeled large-scale warming impacts on summer California coastal-cooling trends. *J. Geophys. Res.,* **116,** D20114, doi:10.1029/2011JD015759.

Leroyer, S., S. Belair, and J. Mailhot, 2011: Microscale numerical prediction over Montreal with the Canadian External Urban Modeling System. *J. Appl. Meteor. Climatol.,* **50,** 2410–2428.

Li, D., and E. Bou-Zeid, 2011: Coherent structures and the dissimilarity of turbulent transport of momentum and scalars in the unstable atmospheric surface layer. *Bound.-Layer Meteor.,* **140,** 243–262.

——, ——, and H. De Bruin, 2012: Monin–Obukhov similarity functions for the structure parameters of temperature and humidity. *Bound.-Layer Meteor.,* **145,** 45–67.

——, ——, M. L. Baeck, S. Jessup, and J. A. Smith, 2013: Modeling land surface processes and heavy rainfall in urban environments: Sensitivity to urban surface representations. *J. Hydrometeor.,* **14,** 1098–1118.

Meehl, G. A., and C. Tebaldi, 2004: More intense, more frequent, and longer lasting heat waves in the 21st century. *Science,* **305,** 994–997.

Ohashi, Y., and H. Kida, 2002: Local circulations developed in the vicinity of both coastal and inland urban areas: A numerical study with a mesoscale atmospheric model. *J. Appl. Meteor.,* **41,** 30–45.

Oke, T. R., 1982: The energetic basis of the urban heat-island. *Quart. J. Roy. Meteor. Soc.,* **108,** 1–24.

Oleson, K. W., G. B. Bonan, J. Feddema, and T. Jackson, 2011: An examination of urban heat island characteristics in a global climate model. *Int. J. Climatol.,* **31,** 1848–1865.

Robine, J. M., S. L. K. Cheung, S. Le Roy, H. Van Oyen, C. Griffiths, J. P. Michel, and F. R. Herrmann, 2008: Death toll exceeded 70,000 in Europe during the summer of 2003. *C. R. Biol.,* **331,** 171–178, doi:10.1016/j.crvi.2007.12.001.

Sailor, D. J., 2011: A review of methods for estimating anthropogenic heat and moisture emissions in the urban environment. *Int. J. Climatol.,* **31,** 189–199.

Skamarock, W. C., and J. B. Klemp, 2008: A time-split nonhydrostatic atmospheric model for weather research and forecasting applications. *J. Comput. Phys.,* **227,** 3465–3485.

Solomon, S., D. Qin, M. Manning, Z. Chen, M. Marquis, K. Averyt, M. Tignor, and H. L. Miller Jr., Eds., 2007: *Climate Change 2007: The Physical Science Basis.* Cambridge University Press, 996 pp.

Stull, R. B., 1988: *An Introduction to Boundary Layer Meteorology.* Kluwer Academic, 670 pp.

Talbot, C., E. Bou-Zeid, and J. Smith, 2012: Nested mesoscale large-eddy simulations with WRF: Performance in real test cases. *J. Hydrometeor.,* **13,** 1421–1441.

Tan, J. G., and Coauthors, 2010: The urban heat island and its impact on heat waves and human health in Shanghai. *Int. J. Biometeor.,* **54,** 75–84.

Wan, Z. M., 2008: New refinements and validation of the MODIS land-surface temperature/emissivity products. *Remote Sens. Environ.,* **112,** 59–74.

Wang, Z. H., E. Bou-Zeid, S. K. Au, and J. A. Smith, 2011a: Analyzing the sensitivity of WRF's single-layer urban canopy model to parameter uncertainty using advanced Monte Carlo simulation. *J. Appl. Meteor. Climatol.,* **50,** 1795–1814.

——, ——, and J. A. Smith, 2011b: A spatially analytical scheme for surface temperatures and conductive heat fluxes in urban canopy models. *Bound.-Layer Meteor.,* **138,** 171–193.

——, ——, and ——, 2012: A coupled energy transport and hydrological model for urban canopies evaluated using a wireless sensor network. *Quart. J. Roy. Meteor. Soc.,* doi: 10.1002/qj.2032, in press.

Yeh, G. T., and W. Brutsaert, 1971a: A solution for simultaneous turbulent heat and vapor transfer between a water surface and the atmosphere. *Bound.-Layer Meteor.,* **2,** 64–82.

——, and ——, 1971b: Numerical solution of two dimensional steady-state turbulent transfer equation. *Mon. Wea. Rev.,* **99,** 494–500.

Zhang, D. L., Y. X. Shou, R. R. Dickerson, and F. Chen, 2011: Impact of upstream urbanization on the urban heat island effects along the Washington–Baltimore corridor. *J. Appl. Meteor. Climatol.,* **50,** 2012–2029.

Zhou, Y., and J. M. Shepherd, 2010: Atlanta's urban heat island under extreme heat conditions and potential mitigation strategies. *Nat. Hazards,* **52,** 639–668.